Revision 1

A large spectral survey of small lunar craters: Implications for the composition of the lunar mantle

Paul G. Lucey[1], Jessica A. Norman[1], Sarah T. Crites[1,2], G. Jeffrey Taylor[1], B. Ray Hawke[1], Myriam Lemelin[1,2]

[1]Hawaii Institute of Geophysics and Planetology, University of Hawaii at Manoa, 1680 East West Road, Honolulu HI 96822, USA

[2] Department of Geology and Geophysics, University of Hawaii at Manoa, 1680 East West Road, Honolulu HI 96822, USA

Abstract

A global spectral survey of 4506 immature craters with diameters less than 1 km was carried out using near-IR data from the Kaguya Spectral Profiler in order to characterize the composition of the lunar megaregolith. On the basis of band minima and radiative transfer mixing models, small crater spectra fall into three groups: 1) mare basalts with strong absorptions at relatively long wavelengths indicating high ratios of high to low Ca pyroxene; 2) norites containing about 50% plagioclase and with pyroxene assemblages dominated by low-Ca pyroxene that occur within the South Pole-Aitken Basin (SPA), near Apollo 14 and other locations near Imbrium Basin, and three major cryptomaria deposits;

Always consult and cite the final, published document. See http://www.minsocam.org or GeoscienceWorld

and 3) noritic anorthosites occurring within the Feldspathic Highlands Terrane containing about 20 wt% pyroxene with a pyroxene assemblage containing exclusively very low Ca pyroxene. Very few pure anorthosites are present in this survey and there are no occurrences of pyroxene-poor olivine-rich assemblages. Models of the composition of basin ejecta incorporate large amounts of mantle material and the spectral results require that that the sampled mantle is orthopyroxenite. Basin depth-diameter ratios used in the models required to match the measured composition are consistent with prior estimates for the largest basins. The composition found in the SPA and Imbrium regions are consistent with mafic impact melt breccias or basaltic impact melts of basin origin. For SPA we model this composition and find it requires an extremely low impact angle. While this is consistent with prior work on an oblique impact for the SPA event, a more robust solution invokes the production of norite in impact melt seas.

Introduction

One of the more intriguing observations in lunar remote sensing was made by Pieters 1986 who noted a significant difference between the noritic composition of the uppermost crust inferred from spectra of small craters, and diverse mineral assemblages observed in central peaks. Pieters indicated that it seemed not possible to arrive at the noritic composition by mixing the observed deeper compositions and proposed a number of hypotheses to account for the observations. These included compositional gradients imposed on the crust during magma ocean crystallization, post-magma ocean igneous intrusions into the crust, or deposition on the surface of material deeply excavated by major impact basins.

Always consult and cite the final, published document. See http://www.minsocam.org or GeoscienceWorld

47

48 In Pieters 1986 the small crater sample comprised craters 5 km or smaller, based
49 principally on the spatial resolution limitations of the groundbased spectroscopic
50 technique then available. With the abundant new spectral data now available we can
51 expand the sample of small craters to all longitudes, and include smaller craters. Pieters
52 acknowledged that her inclusions were based on a relatively small sample; expanding that
53 sample is the goal of this paper.

54

55 We present the results of spectral analysis of about 2700 lunar highland craters occurring
56 at latitudes within 50 degrees of the equator and at all longitudes. We analyze these data
57 with an empirical comparison of the spectra of the craters with the well-documented
58 spectral and compositional data of the Lunar Soils Characterization Consortium (LSCC)
59 data (Taylor et al, 2001, 2010) and with radiative transfer mixing models. We place these
60 results into context using models of basin excavation and basin melt formation to test the
61 hypothesis that the materials of this crater population represent basin ejecta, or basin
62 impact melt.

63

64 Data

65

66 Visible and near-infrared spectra from the Japanese Space Agency (JAXA) SELENE (Kaguya)
67 Spectral Profiler (SP) were used for the survey. SP obtained a global sample of spectra of
68 the lunar surface at a resolution of ~550 m from 0.5 to 2.4 μm in the form of single pixel,
69 largely nadir profiles along the track of the polar orbit of the SELENE satellite (Haruyama

Always consult and cite the final, published document. See http://www.minsocam.org or GeoscienceWorld

et al. 2008; Matsunaga et al. 2008; Yamamoto et al. 2010). During the course of the SELENE mission the orientation of the plane of the satellite orbit with respect to the Moon-sun line--the beta angle--varied widely so optimal lighting conditions where the solar incidence angle is at a minimum occur only in portions of the data (the illumination history of the SP experiment is given in Yokota et al. 2011). Numbered by orbit ("revolution" in JAXA's terminology), revolutions between 4000 and 5000 were particularly well-illuminated so this survey used that range of data. Of the 1000 orbits in this range, 467 were used for the survey comprising approximately five million spectra. The data were photometrically corrected using the equations of Yokota et al. 2011 using the "highland" photometric parameters.

To detect the desired craters for this survey, the first criterion was to cull out mature locations from the data. The space weathering parameter OMAT (Lucey et al 2000) was computed from the data using the constants provided in that paper, and a cutoff of 0.25 was applied to the data to isolate candidate immature locations. OMAT includes apparent reflectance as an input parameter and so is sensitive to variations in that quantity due to topographic shading. To minimize that effect and also to maximize signal-to-noise ratio, analysis was also confined to latitudes within 50 degrees of the equator. This culling resulted in a total of 37,870 candidate spectra with high OMAT values indicating likely immature locations. Because mass wasting and large recent craters can produce fresh surfaces not associated with small craters, and the remaining topographic shading can cause OMAT artifacts on sun-facing slopes, each candidate location was visually inspected using Kaguya Multiband Imager (MI) data and classified as a small crater, large crater or

Always consult and cite the final, published document. See http://www.minsocam.org or GeoscienceWorld

other geologic feature. This resulted in identification of 4506 individual immature craters less than 1 km in diameter. For the many of these craters more than one SP spectrum occurs within one crater radius from the rim so the entire data set comprises 8184 individual spectral measurements. The global distribution of these small crater samples is shown in Figure 1. Along with OMAT we also computed FeO using the equations of Lawrence et al. 2000. Using FeO as a way to discriminate mare craters from highland craters, the data contain about 2700 non-mare craters on the basis of FeO contents less than 12 wt.%.

Analysis

Two methods are applied to analyze these data: estimation of the average pyroxene chemistry, and deriving modal abundance of the major minerals. We estimate pyroxene chemistry by deriving the minimum position of the 1-um band due to iron in mafic silicates and comparing this to data from the Lunar Soils Characterization Consortium (LSCC). In most lunar soils the 1-μm band minimum is related to the pyroxene chemistry because of the dominance of lunar soils spectra by pyroxene. While the band position is affected to some degree by iron content, the largest effect is due to the average calcium content (Adams 1974; Hazen et al. 1978; Cloutis 1985; Klima et al. 2007, 2011; Denevi et al. 2007). In the complex mixture that is lunar soils, the average pyroxene chemistry can be expressed as the ratio of low Ca pyroxene to total pyroxene as lunar soils typically contain more than one pyroxene. The LSCC data show a clear correlation of low Ca pyroxene to

Always consult and cite the final, published document. See http://www.minsocam.org or GeoscienceWorld

115 total pyroxene with band minimum, and we will quantify and use this relationship to
116 interpret the small crater database.
117
118 The position of the minimum in this study is determined first by removing a straight-line
119 continuum by division from each spectrum by defining a line from reflectance values at the
120 wavelengths of 0.75 and 1.5 μm. We then locate the minimum spectral channel between
121 the continuum wavelengths, and finally fit the continuum-removed spectrum with a 2nd
122 order polynomial within fifty nanometers of the minimum spectral channel. We report the
123 minimum value of that polynomial as the band minimum. The fitting processing mitigates
124 the quantization that would occur if only the minimum spectral channel were taken as the
125 actual minimum. In a minority of cases a portion of the spectrum near 1.1 μm exceeds
126 unity in spectra with the continuum as defined removed; in these cases a three point
127 continuum is defined using a parabola as the continuum function and the minimum derived
128 as above in the 1-μm region.
129
130 To directly connect the band minima of the small craters to those of to lunar samples, we
131 compare these results to the band minima of a portion of the Lunar Soils Characterization
132 Consortium (LSCC) data. These data comprise 19 soils spanning the full range of
133 composition present at the Apollo landing sites. These samples were sieved into several
134 size fractions; we use the 10-20 μm size fraction as this fraction was found to be most
135 similar to the spectra of the bulk soil (Pieters et al. 1993). In the LSCC data set, pyroxenes
136 are classified into four types: high and low iron clinopyroxene, pigeonite (low Ca
137 clinopyroxene) and orthopyroxene. For this study we classify pigeonite and orthopyroxene

Always consult and cite the final, published document. See http://www.minsocam.org or GeoscienceWorld

as “low Ca pyroxene” and the two more calcic pyroxene types as “high Ca pyroxene.” We note here that we will be using the term "norite" for rocks containing pyroxene assemblages dominated by with low-Ca pyroxene chemistries and gabbro for rocks containing high-Ca pyroxene chemistries. However, a pigeonite-dominated rock would be technically a gabbro, but spectroscopically, pigeonites resemble orthopyroxenes more than they do clinopyroxenes, even though pigeonites are, structurally, more often monoclinic. We should also note that as will be shown below many of the craters analyzed exhibit band minima too short to contain significant pigeonite.

As expected, the data from LSCC shows a correlation between the band minimum and the relative abundance of low and high Ca pyroxene (Figure 2, r=0.88) that we use to construct a calibration equation. A simple regression between these quantities to produce a predictive equation gives rise to unrealistically ~~short~~ long wavelengths for mixtures dominated by low Ca pyroxene (that is, band minima near 0.9 μm), undoubtedly due to the relatively small sample size and range of the parameter in these data. To arrive at a calibration consistent with prior measurements of the spectral properties of pyroxene, we fixed the band position of pure low Ca pyroxene at 0.905 μm corresponding to the shortest wavelength observed in that mineral (Klima et al. 2007, 2011), and fit the LSCC data forced through that data point. With this constraint, the predictive equation for pyroxene composition is:

Low Ca Pyroxene/Total Pyroxene = 6.7 x (band minimum - 0.905)

Always consult and cite the final, published document. See http://www.minsocam.org or GeoscienceWorld

Applying this equation to the LSCC data, the uncertainty in prediction of low-Ca pyroxene / total pyroxene is 0.085 on a scale of 0 to 1. This equation will form the basis for the interpretation of the small crater band minima.

Figure 3 shows the histogram of band minima for the small crater data set, showing a distinct bimodal distribution representing the difference in pyroxene composition between mare and highland. Mare craters contain high-Ca pyroxene as indicated by the mode near 0.97 μm, and highland craters contain more low-Ca pyroxene as indicated by the mode near 0.91 μm. To investigate spatial variations in this parameter, we interpolated the data to a gridded product at 1 degree resolution shown in Figure 4. The mare-highland dichotomy in average pyroxene chemistry is evident, but there are also strong variations outside the maria, with the largest distinction being the difference between the interior of the South Pole-Aitken basin (SPA) and the more feldspathic highlands. This gridded product includes averaging; in Figure 5 we present histograms of the band minima histograms of spectra occurring within SPA and the Feldspathic Highland Terrane north of SPA as defined by Jolliff et al. 2000. The two terranes differ distinctly in the position of their band minima, with the FHT having a mean band minimum wavelength of 0.906 +/- .008 and SPA showing a mean of 0.922 +/- .010. To further understand the distribution of these distinct units on the basis on their minima, (Figure 6) shows the locations of spectra with band minima within one sigma of the mean of those of the interior of SPA and the FHT. Spectra with SPA-like minima occur in the vicinity of Imbrium and a significant cluster near the Apollo 14 site. Clusters also appear at the major cryptomaria of Schiller-Schickard, Balmer-Kapteyn and Lomonosov-Fleming. Spectra with minima close to those in the FHT

Always consult and cite the final, published document. See http://www.minsocam.org or GeoscienceWorld

184 are somewhat more uniformly distributed, but almost absent in the Imbrium region and
185 within SPA. There is little geographic overlap in the distributions of the two spectral types.
186
187 The average spectra of the small craters in these terranes are typical of relatively fresh
188 feldspathic and mafic highland material (Figure 7). The FHT spectra show weak 1-μm
189 bands with about 5% deep mafic bands, and a strong shoulder near 1.25 μm due to
190 feldspar. These correspond to the spectral type N-1 of Pieters 1986 that she interpreted to
191 be "...feldspathic, minor low-Ca pyroxene (orthopyroxene) component..." The SPA spectra
192 have about twice the band depth indicating a higher abundance of mafic minerals, and also
193 exhibit a shoulder at 1.25 μm due to feldspar, and correspond to spectral type N-3 of
194 Pieters 1986. This type was interpreted to be: "...noritic composition; minor Ca pyroxene ..."
195 Using the LSCC-derived calibration, the low Ca pyroxene / total pyroxene ratio of the small
196 crater population of the FHT is 0.99 +/- .05, whereas the small craters within SPA and
197 regions with similar spectra have a value of 0.88 +/- .07. The implications of these results
198 are discussed below.
199
200 While the pyroxene chemistry is of high interest, the abundance of the major minerals is
201 also important and we derive these using radiative transfer modeling. Our analysis is
202 based on the work of Hapke (1981, 1993, 2001) and versions of our implementation has
203 been presented in Lucey, 1998; Clark et al. 2001; Lawrence and Lucey 2007; Denevi et al.
204 2008; Cahill et al. 2010. For this study we developed an improved mineral abundance
205 algorithm that returns mineral abundances with under 10 % accuracy (Figure 7). The
206 Supplement/Appendix describes the algorithm used and the basis for its improvement.

Always consult and cite the final, published document. See http://www.minsocam.org or GeoscienceWorld

Using the improved algorithm, we find significant differences in the estimated mineralogy between craters of the FHT and those of SPA. Like the empirical band minimum analysis, we find that the FHT spectra show higher abundances of low-Ca pyroxene than found in spectra occurring within SPA (and similar spectra), and in fact the models return almost no high Ca pyroxene in the FHT and a few percent within SPA.

Mineralogical anomalies are very rare. In the entire small crater database of 8184 spectra, only 13 have band minima near 1.25 μm indicating the presence of pure anorthosite (that is exhibit weak or absent pyroxene bands) and all but three of these are very near the rings of Crisium. There are no analogies to the central peaks of Copernicus (Pieters 1982) or the olivine-rich locations identified by Yamamoto et al. 2010 where pyroxene is a minor component.

Discussion

The extensive sampling here underscores and strengthens the observations made by Pieters (1986). The spectral character of the small crater population of the FHT, away from SPA, Imbrium and cryptomaria is exclusively noritic in the strict sense, with no evidence for significant high Ca pyroxene. The absorption band minima exhibited by these spectra are uniformly at very short wavelengths (Figure 5) indicating that this material contains only orthopyroxene as a mafic phase.

Always consult and cite the final, published document. See http://www.minsocam.org or GeoscienceWorld

The FHT composition can be modeled as mechanical mixing and emplacement of ejecta composed of pure anorthosite crust with an underlying orthopyroxenite mantle. Following the method detailed in Crites et al. (this volume) we model the crustal composition of the FHT as the average of the ejecta of the 43 largest lunar basins identified by Spudis (1993), including SPA. The ejecta composition of each basin was modeled based on the volume percent of mantle and crust excavated following the basin ejecta volume calculations of Spudis (1993). In this approach, the final composition is controlled by the diameter of the basin, the depth/diameter ratio, and the crustal thickness. The ejected volume is treated as a spherical cavity intersecting a spherical moon. The circle defined by the intersecting spheres is taken as the basin transient cavity and its diameter is fixed at the transient cavity diameter estimated for each basin by Petro and Pieters (2004). The depth associated with the depth-diameter ratio is defined as the distance between the deepest point on the excavation cavity sphere and the surface of the lunar sphere directly above this point. The depth-diameter ratio of the excavation cavity is the excavation depth divided by the diameter of the circle representing the transient cavity. This ratio can be varied arbitrarily by adjusting the distance of the excavating sphere from the center of the Moon and the excavating sphere's radius. The Moon is modeled as a shell of pure orthopyroxenite mantle, overlain by a shell of anorthosite, in this case 2% orthopyroxene and 98% plagioclase. Varying depth diameter ratio and crustal thickness allows us to arrive at an average basin ejecta composition matching that of the FHT. Two crustal thicknesses were used, 34 and 43 km from the average crustal thickness estimates of Wieczorek et al. (2013), and these gave rise to basin depth diameter ratios of 0.059 and 0.074 to match the observed composition of the FHT. For context, a wide range of

Always consult and cite the final, published document. See http://www.minsocam.org or GeoscienceWorld

theoretical methods, experiments, and observations agree that for craters ranging in size from centimeters to tens of kilometers, the depth to diameter ratio for the Moon is approximately 1:10 (Croft, 1980, O'Keefe and Ahrens 1993, Wieczorek and Phillips 1999). However, modeled excavation cavities based on gravity data by Wieczorek and Phillips (1999) for the three largest lunar basins (Serenitatis, Imbrium, and SPA) fall off this trend, with the depth:diameter ratios for Serenitatis and Imbrium estimated near 0.05, and for SPA 0.01 or even shallower. Although in our calculations we modify the depth:diameter ratio for all 43 basins, approximately 70% of the total ejecta and over 90% of the mantle material is derived from the 3 largest basins so our results are dominated by these basins, and our relatively shallow depth:diameter ratios are in agreement with the observations of Wieczorek and Phillips (1999). Notably, for a maximum crustal thickness of 60 km observed in the center of the FHT by Wieczorek et al. (2013), a depth:diameter ratio of almost exactly 1:10 produces the FHT composition from an orthopyroxenite mantle and anorthosite crust.

Turning to the spectral type exposed at SPA and elsewhere, the interior of the basin likely exposes abundant impact melt from its formation (e.g. Petro and Pieters, 2004). Based on that assumption, we investigated the ability to arrive at the SPA composition using the same two layer model used above, but this time modeling bulk melt composition. We assume the melt is derived from a spherical volume tangent to the lunar surface that will include proportions of crust and mantle depending on the crustal thickness and the sphere diameter following the method of Vaughan et al. (2013). We calculated the total melt volume for SPA using the scaling relationship derived by Abramov et al. (2012) and the

Always consult and cite the final, published document. See http://www.minsocam.org or GeoscienceWorld

model inputs of Kring et al. (2012) and used that to calculate the size of the melt sphere. We calculated the fraction of crust and mantle material in the melt based on this simple geometry and derived the bulk melt composition based on our two-layer model. We varied the crustal thickness and the angle of the SPA-forming impact and found a narrow range of parameters that could produce the observed SPA norite composition assuming a pure plagioclase crust and an orthopyroxenite mantle. The statistically most likely impact angle of 45 degrees (Melosh 1989) requires an unreasonably thick anorthositic crust of 140 km to match the SPA small crater composition. A highly oblique impact angle of less than 6 degrees is required for our calculations to permit a crustal thickness at or below 60 km, the maximum crustal thickness observed by Wieczorek et al. (2013). This conclusion is consistent with prior work concluding that SPA was likely an oblique impact (e.g. Schultz 1997, Garrick-Bethel and Zuber 2009).

Implications

The problem posed by Pieters (1986) was that the composition of the materials excavated by central peaks, presumably representing a large section of the crust, is not similar to the noritic composition revealed by the small crater population. The work reported here reinforces that problem by showing the apparent compositional difference between the two populations (central peaks of large craters and deposits of small craters) is not an artifact of poor sampling of the small crater population. This apparent conflict is resolved by recognizing that mantle must comprise a large fraction of basin ejecta (as shown by previous work and modeling done above), and that its ultramafic composition will cause it

Always consult and cite the final, published document. See http://www.minsocam.org or GeoscienceWorld

299 to dominate the mafic composition of a mixture of anorthositic crust and ultramafic mantle.
300 The extreme noritic nature of the small crater population requires that montle composition
301 incorporated into basin ejecta must be largely orthopyroxenite.
302
303 This simple two-layer model ignores a crust that may become more mafic with depth. This
304 has been widely hypothesized and assumed (e.g. Ryder and Wood, 1977), and if true would
305 reduce the amount of mantle required in models to account for the observed total mafic
306 content, but also reduce the basin depth:diameter ratios needed to account for the
307 observations to values below all prior estimates (see calculations in Crites et al. this volume
308 that explicitly deal with this case). The extreme noritic composition observed requires that
309 any more mafic lower crust shares the same relatively extreme low-Ca pyroxene
310 mineralogy as the mantle, as there is no evidence for additional mafic components in the
311 small crater data.
312
313 The spectral type exposed at SPA and the Imbrium region likely represents a basaltic
314 impact melt generated by these large impacts. The melts generated by the SPA and the
315 Imbrium impact events were formed from total melting of a large column that extended
316 into the mantle, a composition that explains the mafic nature of these deposits. However,
317 recently Vaughan et al. (2013) have emphasized and demonstrated the potential
318 importance of differentiation of impact melt pools in large basins, and showed that the
319 upper norite layer seen in some impact melt differentiation models is consistent with
320 observations at SPA. The spectral data here are consistent both with a quenched impact
321 melt formed of an orthopyroxenite mantle and an anorthosite crust, and also with

Always consult and cite the final, published document. See http://www.minsocam.org or GeoscienceWorld

differentiation of an impact melt sea, provided the norite layer is thick enough and close enough to the surface to dominate the surface composition. Even in the presence of other styles of differentiation, a quenched crust may be expected atop melt seas, and preserved in this small crater population. The slightly higher Ca content implied by the difference in band minimum position observed between the FHT-like spectra and SPA-like spectra is consistent with a melt formed from orthopyroxene and plagioclase providing a more calcic melt relative to the very low calcium mantle orthopyroxene source that enabled crystallization of a somewhat higher Ca pyroxene than the source. We favor the Vaughn et al. (2013) model of a differentiated melt sheet owing to the need for a quite extreme impact angle to achieve the proper composition without differentiation.

Finally, we note that the common occurrence of SPA-like spectra within major cryptomaria suggest they are unlike more recent mare basalts in pyroxene chemistry as pointed out by Hawke et al. 2005, with our new finding being that their pyroxene assemblage is much less calcic that typical mare basalts. We take the spectral similarity of the cryptomaria to the small craters within SPA to be a coincidence, however, it should be considered that the deposits of these craters may not indicate the presence of unusual mare basalts, but rather are excavated mafic melt sheets.

References

Abramov, O., Wong. S.M., and Kring, D.A. (2012) Differential melt scaling for oblique impacts on terrestrial planets. Icarus, 218, 906-916, doi: 10.1016/j.icarus.2011.12.022.v

Always consult and cite the final, published document. See http://www.minsocam.org or GeoscienceWorld

Adams, J. B. (1974), Visible and near-infrared diffuse reflectance spectra of pyroxenes as applied to remote sensing of solid objects in the solar system, J. Geophys. Res., 79, 4829– 4836.

Britt, D. and Pieters, C. M. Darkening in black and gas-rich ordinary chondrite meteorites: the spectral effects of opaque morphology and distribution. Geochim. Cosmochim. Acta 58, 3905–3919 (1994).

Cahill, J. T., and P. G. Lucey (2007), Radiative transfer modeling of lunar highlands spectral classes and relationship to lunar samples, J. Geophys. Res., 112, E10007, doi:10.1029/2006JE00286

Cahill, J. T. S., P. G. Lucey, K. R. Stockstill-Cahill, and B. R. Hawke (2010), Radiative transfer modeling of near-infrared reflectance of lunar highland and mare soils, J. Geophys. Res., 115, E12013, doi:10.1029/2009JE003500.

Clark, B.E, Lucey, P.G., P Helfenstein, J.F. Bell III, C. Peterson, J. Veverka, T McConnochie, M.S. Robinson, B Bussey, S.L. Murchie, NI Izenberg, and CR Chapman, Space weathering on Eros: Constraints from albedo and spectral measurements of Psyche crater., Meteoritics and Planetary Science, 36, 1617-1637, 2001

Cloutis, E. A. (1985), Interpretive techniques for reflectance spectra of

Always consult and cite the final, published document. See http://www.minsocam.org or GeoscienceWorld

368 mafic silicates, M. S. thesis, Univ. of Hawaii, Honolulu.

369

370 Cloutis, E. A. (2002), Pyroxene reflectance spectra: Minor absorption bands
371 and effects of elemental substitutions, J. Geophys. Res., 107(E6), 5038,
372 doi:10.1029/2001JE001587.

373

374 Croft, S.K. (1980) Cratering flow fields: Implications for the excavation and transient
375 expansion stage of crater formation. Proceedings of the 11th Lunar and Planetary Science
376 Conference, p. 2347-2378.

377

378 Denevi, B. W., P. G. Lucey, E. J. Hochberg, and D. Steutel (2007), Near-infrared optical
379 constants of pyroxene as a function of iron and calcium content, J. Geophys. Res., 112,
380 E05009, doi:10.1029/2006JE002802.

381

382 Denevi, B. W., P. G. Lucey, and S. B. Sherman (2008), Radiative transfer modeling of near-
383 infrared spectra of lunar mare soils: Theory and measurement, J. Geophys. Res., 113,
384 E02003, doi:10.1029/2007JE002929.

385

386 Garrick-Bethell, I., Zuber, M.T., 2009. Elliptical structure of the lunar South
387 Pole-Aitken basin. Icarus 204, 399–408. http://dx.doi.org/10.1016/
388 j.icarus.2009.05.032.

389

Always consult and cite the final, published document. See http://www.minsocam.org or GeoscienceWorld

Hamilton, V. E., and P. R. Christensen, Determining the modal mineralogy of mafic and ultramafic igneous rocks using thermal emission spectroscopy, J. Geophys. Res., 105, 9717-9733, 2000.

Haruyama, J., Matsunaga, T., Ohtake, M., Morota, T., Honda, C., Yokota, Y., Torii, M., Ogawa, Y., the LISM Working Group, 2008. Global lunar-surface mapping experiment using the Lunar
Imager/Spectrometer on SELENE, Earth Planets Space , 60, 243–255.

Hawke, B. R., J. J. Gillis, T. A. Giguere, D. T. Blewett, D. J. Lawrence, P. G. Lucey, G. A. Smith, P. D. Spudis, and G. J. Taylor (2005), Remote sensing and geologic studies of the Balmer-Kapteyn region of the Moon, J. Geophys. Res., 110, E06004, doi:10.1029/2004JE002383.

Hazen, R. M., P. M. Bell, and H. K. Mao (1978), Effects of compositional
variation on absorption spectra of lunar pyroxenes, Proc. Lunar Planet.
Sci. Conf., 9th, 2919– 2934.

King, T. V. V., and W. I. Ridley (1987), Relation of the Spectroscopic Reflectance of Olivine to Mineral Chemistry and Some Remote Sensing Implications, J. Geophys. Res. 92(B11), 11,457-11,469.

Klima, R. L., C. M. Pieters, and M. D. Dyar (2007), Spectroscopy of synthetic

Always consult and cite the final, published document. See http://www.minsocam.org or GeoscienceWorld

Mg-Fe pyroxenes I: Spin-allowed and spin-forbidden crystal field bands in the visible and near-infrared, Meteorit. Planet. Sci., 42, 235–253, doi:10.1111/j.1945-5100.2007.tb00230.x.

Klima, R. L., M. D. Dyar, and C. M. Pieters (2011), Near-infrared spectra of clinopyroxenes: Effects of calcium content and crystal structure, Meteorit. Planet. Sci., 46, 379–395, doi:10.1111/j.1945-5100.2010.01158.x.

Kring, D.A., Abramov, O., and Marchi, S. (2012) Impact melt production during the basin-forming epoch. Lunar and Planetary Science Conference XLIII, Abstract #1615.

Lawrence, D. J., W.C. Feldman, R.C. Elphic, R.C. Little, T.H. Prettyman, S. Maurice, P.G. Lucey, A. B. Binder, Iron abundances on the lunar surface as measured by the Lunar Prospector gamma-ray and neutron spectrometers Journal of Geophysical Research, VOL. 107, NO. E12, 5130, doi:10.1029/2001JE001530, 2002

Lawrence, S.J. and P. G. Lucey, Radiative transfer mixing models of meteoritic assemblages, Journal of Geophysical Research (Planets) doi:10.1029/2006JE002765, 2007

Lucey, P.G. Model near-infrared optical constants of olivine and pyroxene as a function of iron content, J. Geophys. Res.,103, E1, pp1703-1714, 1998.

Always consult and cite the final, published document. See http://www.minsocam.org or GeoscienceWorld

435 Lucey, P.G and S.K. Noble, Experimental Test of a Radiative Transfer Model of the Optical
436 Effects of Space Weathering , Icarus (2008), doi: 10.1016/j.icarus.2008.05.008
437
438 Lucey, P.G. and M.A. Riner, The optical effects of small iron particles that darken but do not
439 redden: Evidence of intense space weathering on Mercury, Icarus, Volume 212, Issue 2, p.
440 451-462, 2011, doi:10.1016/j.icarus.2011.01.022
441
442 Lucey, P.G., and M.A. Riner (2011), The optical effects of small iron particles that darken but
443 do
444 not redden: Evidence of intense space weathering on Mercury, Icarus, 212(2), 451-462.
445
446 Lucey, P. G., and S. K. Noble (2008), Experimental test of a radiative transfer
447 model of the optical effects of space weathering, Icarus, 197, 348–353.
448
449 Lucey, P.G., D.T. Blewett, G. J. Taylor, and B.R. Hawke, Imaging the maturity of the lunar
450 surface, J. Geophys. Res, 105, E8, 20297-20305, 2000
451
452 Matsunaga, T., Ohtake, M., Haruyama, J., Ogawa, Y., Nakamura, R., Yokota, Y., Morota, T.,
453 Honda, C., Torii, M., Abe, M., Nimura, T., Hiroi, T., Arai, T., Saiki, K., Takeda, H., Hirata, N.,
454 Kodama, S., Sugihara, T., Demura, H., Asada, N., Terazono, J., Otake, H., (2008). Discoveries
455 on the lithology of lunar crater central peaks by SELENE Spectral Profiler, Geophys. Res.
456 Lett., 35 , L23201.
457

Always consult and cite the final, published document. See http://www.minsocam.org or GeoscienceWorld

458 Nakamura, R.; Yamamoto, S.; Matsunaga, T.; Ishihara, Y.; Morota, T.; Hiroi, T.; Takeda, H.;
459 Ogawa, Y.; Yokota, Y.; Hirata, N.; Ohtake, M.; Saiki, K. (2012). "Compositional evidence for an
460 impact origin of the Moon's Procellarum basin". Nature Geoscience 5 (11): 775.
461 doi:10.1038/NGEO1614
462
463 Noble, S. K., C. M. Pieters, and L. P. Keller (2007), An experimental
464 approach to understanding the optical effects of space weathering, Icarus,
465 192, 629–642.
466
467 O'Keefe, J.D. and Ahrens, T.J. (1993) Planetary cratering mechanics. Journal of Geophysical
468 Research, 98, 17,011-17,028.
469
470 Petro, N. E., and C. M. Pieters (2004), Surviving the heavy bombardment: Ancient material
471 at the surface of South Pole-Aitken Basin, J. Geophys. Res., 109, E06004, doi:
472 10.1029/2003JE002182.
473
474 Petro, N.E. and Pieters, C.M. (2008) The lunar-wide effects of basin ejecta distribution on
475 the early megaregolith. Meteoritics and Planetary Science, 43, 1517-1529.
476
477 Pieters, C. M. (1986), Composition of the lunar highland crust from near-infrared
478 spectroscopy, Reviews of Geophysics and Space Physics, 24, 557-578.
479

Always consult and cite the final, published document. See http://www.minsocam.org or GeoscienceWorld

Pieters, C. M., E. M. Fischer, O. Rode, and A. Basu (1993), Optical effects of space weathering: The role of the finest fraction, J. Geophys. Res., 98, 20,817– 20,824.

Ryder G. and J. A. Wood: Serenitatis and Imbrium impact melts: Implications for large-scale layering in the lunar crust. Proc. Lunar Sci. Conf. 8th, 655-668, 1977

Schultz, P.H. (1997) Forming the South Pole-Aitken Basin: The extreme games. Proceedings of the 27th Lunar and Planetary Science Conference, p. 1259-1260.

Stoffler, D., Knoll, H.-D., Marvin, U.B., Simonds, C.H., and Warren, P.H. (1980) Recommended classification and nomenclature of lunar highland rock—A committee report. In J.J. Papike and R.B. Merrill, Eds., Proceedings of the Conference on the Lunar Highland Crust, p 51-70, Pergamon Press

Taylor, L. A., C. Pieters, A. Patchen, D.-H. S. Taylor, R. V. Morris, L. P. Keller, and D. S. McKay (2010), Mineralogical and chemical characterization of lunar highland soils: Insights into the space weathering of soils on airless bodies, J. Geophys. Res., 115, E02002, doi:10.1029/2009JE003427.

Taylor, L. A., C. M. Pieters, L. P. Keller, R. V. Morris, and D. S. McKay (2001), Lunar Mare Soils: Space weathering and the major effects of surface-correlated nanophase Fe, J. Geophys. Res., 106(E11), 27985–27999, doi:10.1029/2000JE001402.

Always consult and cite the final, published document. See http://www.minsocam.org or GeoscienceWorld

503 Trang, D., P. J. Isaacson, and 4 co-authors (2013), Near-infrared optical constants of
504 naturally
505 occurring olivine and synthetic pyroxene as a function of mineral composition, J. Geophys.
506 Res., 118, doi:10.1002/jgre.20072.
507
508 Vaughan, W.M., Head, J.W., Wilson, L., and Hess, P.C. (2013) Geology and petrology of
509 enormous volumes of impact melt on the Moon: A case study of the Orientale basin impact
510 melt sea. Icarus, 223, 749-765, doi: 10.1016/j.icarus.2013.01.017.
511
512 Wieczorek, M.A. and Phillips, R.J. (1999) Lunar multiring basins and the cratering process.
513 Icarus, 139, 246-259.
514
515 Yamamoto, S. et al., 2010. Possible mantle origin of olivine around lunar impact
516 basins detected by SELENE. Nat. Geosci. 3, 533–536. http://dx.doi.org/10.1038/
517 ngeo897.
518
519 Yokota, Y., T. Matsunaga, M. Ohtake, J. Haruyama, R. Nakamura, S. Yamamoto, Y. Ogawa, T.
520 Morota, C. Honda, K. Saiki, K. Nagasawa, K. Kitazato, S. Sasaki, A. Iwasaki, H. Demura, N.
521 Hirata, T. Hiroi, R. Honda, Y. Iijima, H. Mizutani, Lunar photometric properties at
522 wavelengths 0.5–1.6μm acquired by SELENE Spectral Profiler and their dependency on
523 local albedo and latitudinal zones, Icarus, Volume 215, Issue 2, 2011, pp 639-660, ISSN
524 0019-1035, http://dx.doi.org/10.1016/j.icarus.2011.07.028.
525

Always consult and cite the final, published document. See http://www.minsocam.org or GeoscienceWorld

526

527

528

Always consult and cite the final, published document. See http://www.minsocam.org or GeoscienceWorld

529

Table 1. Composition Summary of Highland Spectral Units

	FHT	SPA
Rock Type (Stoffler et al. 1980)	Noritic Anorthosite	Norite
Plagioclase	80.4% +/- 5	56.4% +/- 17
Pyroxene	19.6% +/- 5	41.6% +/- 14
Olivine	0.03%* +/- 1	1.9%* +/- 3
Low Ca Pyroxene/Total	0.99 +/- .01	0.95 +/- .07

Always consult and cite the final, published document. See http://www.minsocam.org or GeoscienceWorld

530 Appendix

531

532 We use a mineral abundance extraction algorithm similar to that used by Cahill et al. 2007.
533 Spectrum libraries are computed for the system plagioclase, low- Ca pyroxene, high-Ca
534 pyroxene, olivine, and nanophase iron of two sizes with different optical effects. The
535 foundation of the compositions are the ternary system of olivine and the two pyroxenes
536 computed at 10% intervals for a total of 66 compositions. These compositions are then
537 mixed with plagioclase at 1% intervals from 0-100% plagioclase for a total of 6600
538 compositions. These compositions in turn are mixed with seven amounts of nanophase
539 iron to simulate space weathering effects. Nanophase iron includes optically small material
540 modeled by ("submicroscopic iron") Hapke 2001 and studied by Noble et al. 2007 and
541 Noble and Lucey (2008), and larger nanophase iron that we call Britt-Pieters particles
542 (Lucey and Riner (2011), Britt and Pieters (1994)) that are an important darkening phase
543 in lunar soils. The abundances of these two components are matched to the measured
544 abundances of these phases in the LSCC soils. For simplicity the abundance of the two sizes
545 are linked by the relationship Britt-Pieters (wt. %) = 2* submicroscopic iron (wt. %) that
546 causes the libraries to occupy the same spectral space as the LSCC data in terms of
547 reflectance and continuum slope. We remove a continuum from all of the model spectra
548 (6600x7) and from the unknown spectrum (for example, one of the LSCC spectra) and we
549 find the closest spectral match and use the composition associated with that model as the
550 mineral composition of that spectrum.

551

Always consult and cite the final, published document. See http://www.minsocam.org or GeoscienceWorld

552 The comparison between the libraries and the spectrum under analysis is an evenly
553 weighted average of the correlation of the library and target spectra after removal of a
554 continuuum, and the sum of the absolute value of the total of the difference between the
555 library and target spectra. The correlation metric emphasizes the similarity in the shape of
556 the spectrum, while the difference metric includes band intensity as an important
557 parameter.
558
559 We plot the result of exercising the mineral mapping algorithm in Figure A1 showing there
560 is a poor correlation of the model and measured mineralogy (greater than 20 wt. % error).
561 However, the behavior of the model against individual minerals provides clues to its
562 shortcomings. The low correlation is due to systematic over and under-prediction of
563 specific minerals, for example, olivine is greatly overestimated. Furthermore, we find that
564 forward modeling of the LSCC compositions (using the LSCC compositions as inputs to
565 compute a reflectance spectrum) produces a set of spectra that do not match the observed
566 trend of band minimum vs the ratio of low-Ca to total pyroxene (Figure A2).
567
568 Successful estimates of relative abundance of minerals in an assemblage using a mixing
569 model requires at the minimum that the relative intensities of the bands of the
570 endmembers accurately reflect the relative intensities of the bands in the unknown spectra.
571 An error in the relative intensities will give rise to an error in estimated abundance. For
572 example, if an endmember intensity is strong relative to the intensity of that component in
573 the mixture undergoing analysis, then the abundance of that component will be
574 underestimated because a lower abundance is adequate to match the band strenght of the

Always consult and cite the final, published document. See http://www.minsocam.org or GeoscienceWorld

575 target spectrum than is actually present. While significant attention has been paid to
576 determining the optical constants of the rock forming minerals within the major mineral
577 classes, especially olivine and pyroxene (Trang et al. 2012;, Denevi et al. 2006) little work
578 has been done to calibrate between classes of minerals. Furthermore, even within mineral
579 classes there are large discrepancies between optical constant intensities derived from
580 sample sets prepared by different investigators. The best documented case was presented
581 by Trang et al.2012 who showed that there is a factor of four discrepancy between the
582 derived band intensities using the data of King and Ridley (1987) vs the data of Sunshine
583 and Pieters [1998] . Interestingly, Sunshine and Pieters [1998] analyzed both of these data
584 sets using MGM, and found they were completely consistent with respect to the absorption
585 band parameters width and center, and even the relative intensities of the olivine bands.
586 However, Trang et al. 2012 showed that the King and Ridley (1987) data are systematically
587 lower in albedo, and exhibit systematically stronger absorption bands than the data
588 presented by Sunshine and Pieters [1998]. Because the optical constants are derived from
589 reflectance spectra using a model that does not include the unknown cause of this
590 difference, the estimated optical constants also contain the corresponding uncertainty in
591 intensity. While the existing optical constants are a starting point in understanding the
592 composition of an unknown spectrum, with testing and validation data the accuracy can be
593 improved by pinning the relative intensities of the endmembers to ground truth. The data
594 set of the LSCC is that ground truth for lunar spectral studies.
595
596 In addition to intensities, the radiative transfer model should also obey observed spectral
597 trends in the validation data set. We find that forward modeling of the LSCC compositions

Always consult and cite the final, published document. See http://www.minsocam.org or GeoscienceWorld

598 using (using the LSCC compositions as inputs to compute a reflectance spectrum) produces
599 a set of spectra that do not match the observed trend of band minimum vs the ratio of low-
600 Ca to total pyroxene (Figure A2) indicating that the low-Ca pyroxene endmember exhibits a
601 band center that is too long in wavelength, and the high-Ca pyroxene endmember exhibits a
602 band center that is too short in wavelength.
603
604 For these reasons, in order to improve the estimation of abundance as characterized by the
605 performance of the algorithm against the LSCC data, we elected to treat the band intensities
606 of the four minerals as free parameters in an optimization. To ameliorate the trend
607 problem shown in Figure A2, we also allowed the pyroxene optical constants to "float" in
608 wavelength. We performed a high fidelity grid search of space defined by the 6 parameters
609 adjusted. We found the best performance with a shift of the low Ca-pyroxene imaginary
610 index spectrum of Lucey 1998 (computed at an Mg-number of 65) by 12.5 nm to shorter
611 wavelengths, and the high-Ca pyroxene imaginary index spectrum by 50 nm to longer
612 wavelengths, in increase in intensity of the olivine imaginary index spectrum by a factor of
613 seven, and that of plagioclase by a factor of two gave rise to this improvement. The
614 intensities of the imaginary index spectra of the two pyroxenes remained unchanged.
615
616 A factor of seven in intensity increase in the olivine intensity (relative to pyroxene) may
617 seem extremely large, however, note Trang et al 2012 documented a factor of four
618 difference in absorption intensity within reported olivine spectra. Furthermore, the olivine
619 was computed at an Mg-number of 65, while the LSCC average olivine composition is
620 somewhat less magnesian. Finally, the fits may be compensating for an systematic

Always consult and cite the final, published document. See http://www.minsocam.org or GeoscienceWorld

621 difference between the olivine and pyroxene in ways not accounted for in the model, for
622 example surface texture or internal scattering, that can affect the reflectance spectrum.
623
624 The result of this optimization was a significant improvement in performance as shown in
625 Figure 8 (main text). The mean error in mineral estimation is 8%, down from the 25%
626 using the original values. Olivine and high-Ca pyroxene are no longer grossly
627 overestimated, and plagioclase shows better correlation. Turning back to the trend of band
628 minimum vs. low-Ca pyroxene over total pyroxene, forward modeled spectra of the LSCC
629 compositions are much more consistent with the LSCC data than the previous effort
630 (though not exact) (Figure A3). The ability of the model to retrieve the LSCC abundances
631 with less than 10% error is similar to the formal error in extraction of Mars compositions
632 from TES data (Hamilton and Christensen, 2000).
633
634
635

Always consult and cite the final, published document. See http://www.minsocam.org or GeoscienceWorld

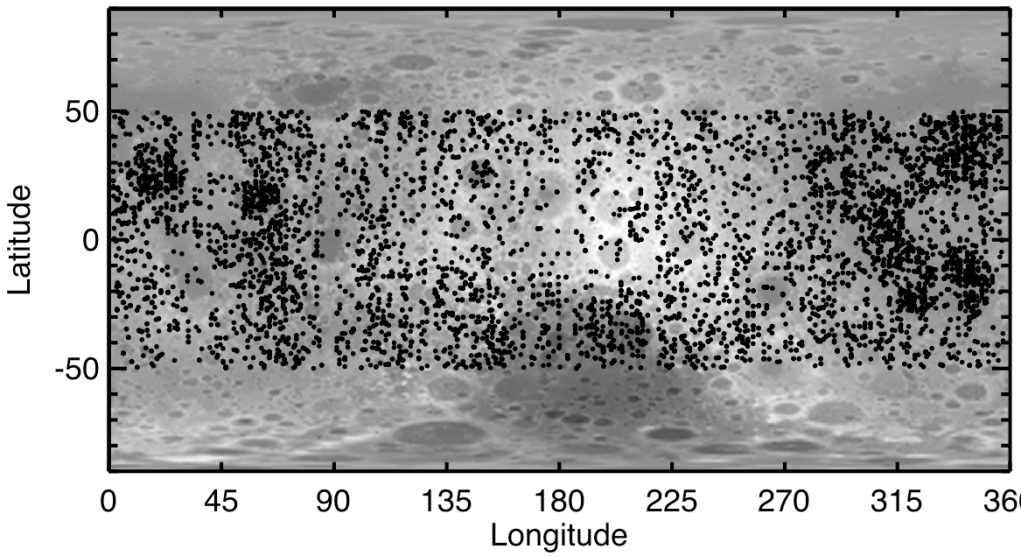

Figure 1. Locations of all craters used in this survey. Background image is Kaguya topography. The greater density of points in the maria reflect the presence of thin regolith permitting the small impacts studied in this work to create abundant fresh material from competent underlying material.

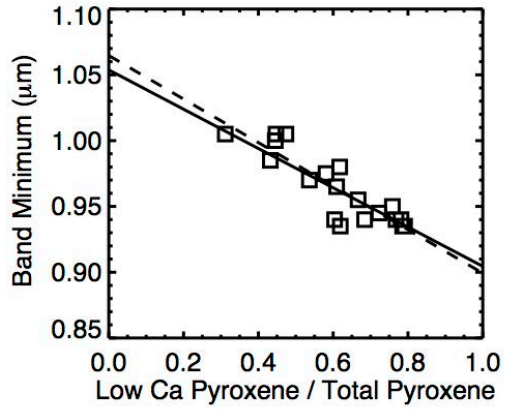

Figure 2. Band minimum vs. ratio of low Ca pyroxene for 19 soils of Taylor et al. 2001, 2010 (squares). The solid line is the linear regression to these data. The dashed line is the fit forced through a value of 0.905 for pure low Ca pyroxene.

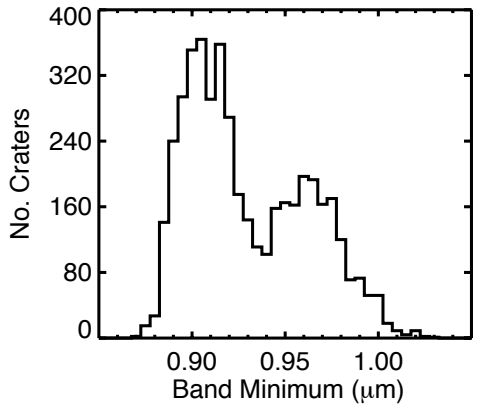

Figure 3. Histogram of band minimum for the small survey crater data set. The peak near 0.97 microns corresponds to the lunar maria, and the peak near 0.9 microns corresponds to the lunar highlands.

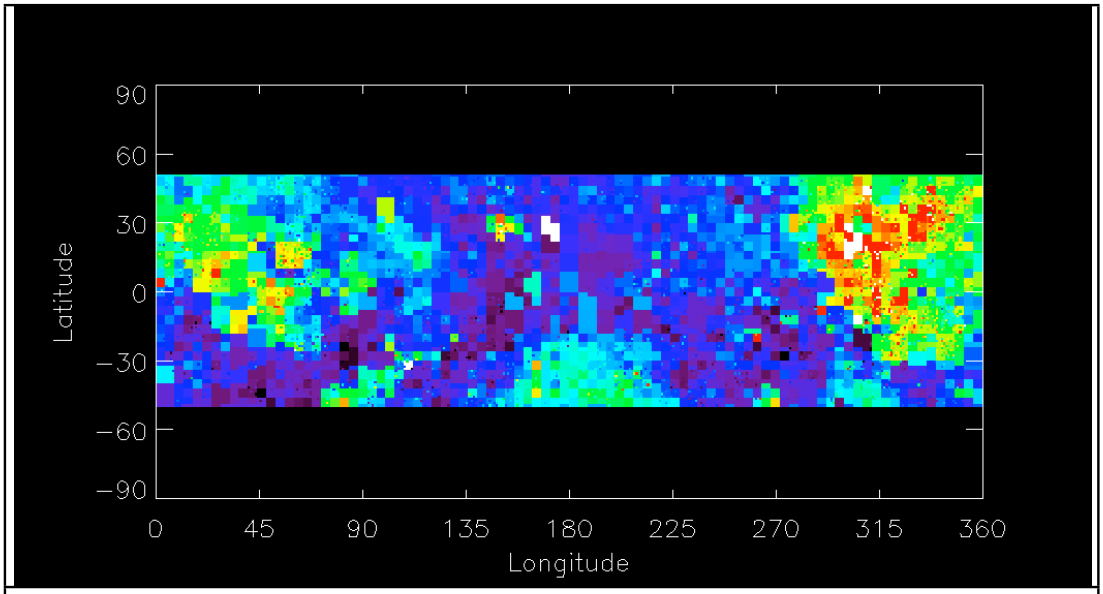

Figure 4. Map of band minimum. Data ranges from 0.9 (black) to 0.97 (white). The long wavelengths exhibited in the maria indicate dominance by high Ca pyroxene. Outside the maria two units are apparent, very short values corresponding to the Feldspathic Highland Terrane (blue tones) and slightly longer wavelengths occurring within South Pole-Aitken Basin and some cryptomaria.

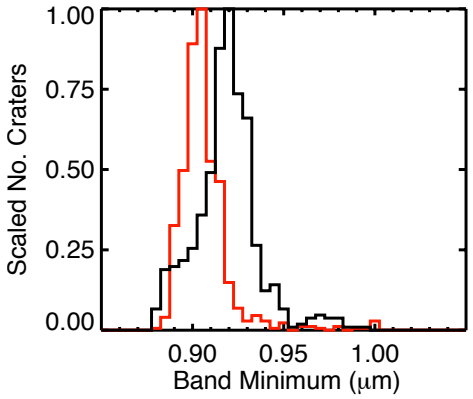

Figure 5. Histogram of band minimum for the Feldspathic Highlands Terrane (red) and South Pole-Aitken Basin (black) illustrating the offset in band minimum, and hence composition. A few small mare exposures occur within both units as seen in the "long tail" of the distribution.

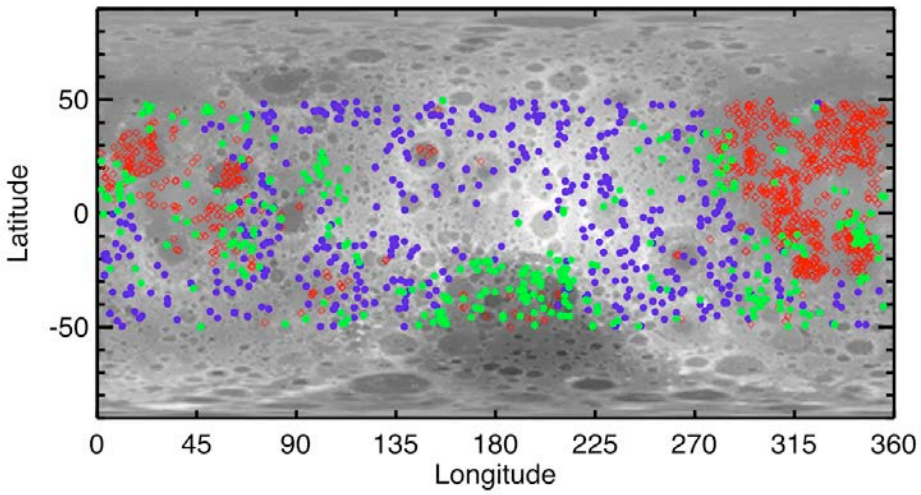

Figure 6. Locations of spectral types based on band minimum. Red diamonds: maria; green dots, spectra with band minima similar to those in South Pole-Aitken Basin; blue dots, spectra with band minima similar to those in the Feldspathic Highlands Terrane.

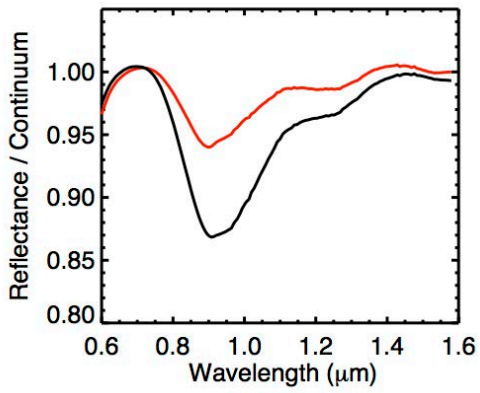

Figure 7. Average spectra of SP-A small craters (black) and FHT small craters (red).

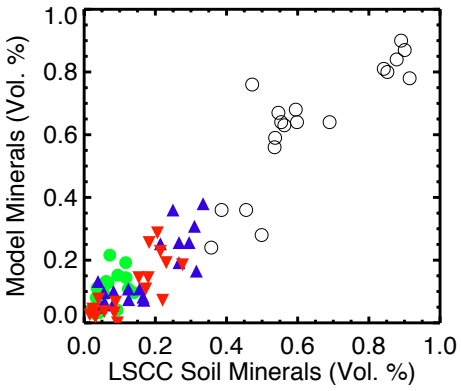

Figure 8. Correlation of measured and modeled LSCC soil mineralogy using the algorithm described employing the algorithm described in the Appendix. Mineral abundance prediction is about with ~ 8 vol % error in predicted mineralogy. Green: olivine; red, high Ca pyroxene; blue, low Ca pyroxene; black circles, feldspar

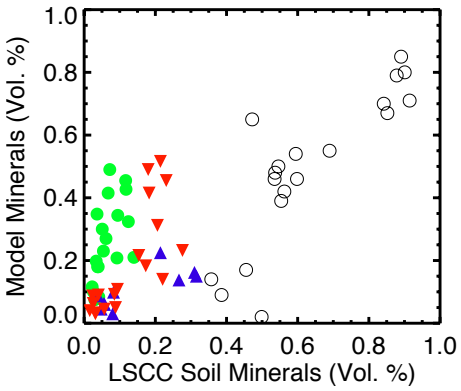

Figure A1. Correlation of measured and modeled LSCC soil mineralogy using the algorithm described. Green: olivine; red, high Ca pyroxene; blue, low Ca pyroxene; black circles, feldspar

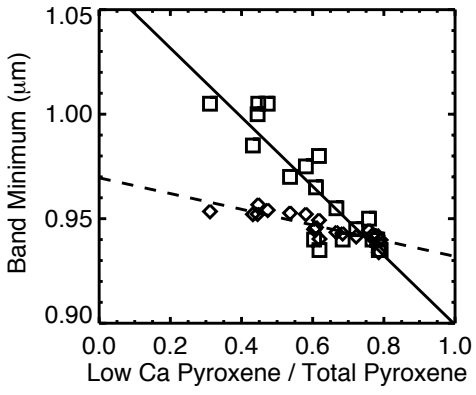

Figure A2. Black squares are the LSCC soils with a regression fit to the data. The diamonds are the locations of spectra computed using the spectral model employing the Lucey 1998 optical constants. The difference in trends is an important contributor to the error in prediction of modal mineralogy

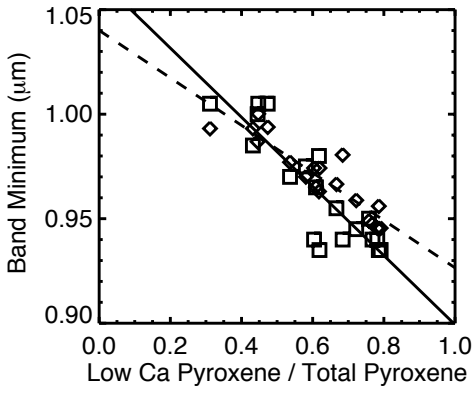

Figure A3. Black squares are the LSCC soils with a regression fit to the data. The diamonds are the locations of spectra computed using the spectral model employing the modified optical constants produced for this project. There is much better overlap between the predicted and measured spectra, and the trends produced by the two data sets.